

# Cosmological model with Gong-Zong Parametrization in $f(R, L_m)$ gravity

Romanshu Garg<sup>1\*</sup>; Tanmoy Chowdhury<sup>2†</sup>; G. P. Singh<sup>1‡</sup>; Farook Rahaman<sup>2§</sup>

<sup>1</sup> Department of Mathematics,  
Visvesvaraya National Institute of Technology, Nagpur, 440010, Maharashtra India.

<sup>2</sup> Departments of Mathematics,  
Jadavpur University, Kolkata 700032, West Bengal, India.

## Abstract

We present the cosmic expansion scenarios in the  $f(R, L_m)$  gravity studied by using the dark energy equation of state (EoS) parameters. We proceed with the specific form of  $f(R, L_m)$  gravity termed as  $f(R, L_m) = \frac{R}{2} + L_m^\alpha$ . We derive the expansion rate in terms of the red-shift for two different forms of EoS parameter. In first model, EoS parameter varies inversely with the redshift and in second model, it involves the exponential form with the redshift. By using the Bayesian methods based on the  $\chi^2$ -minimization technique, the median values of model parameters are determined for the cosmic chronometer(CC) and Joint (CC+Pantheon) data sets. The behavior of fundamental cosmological parameters such as the deceleration parameter, energy density and pressure are thoroughly examined. Additionally, the nature of Statefinder diagnostics and the present age of universe exemplifies the compatibility with the late-time astronomical observations.

**Keywords:**  $f(R, L_m)$  gravity, EoS parameters, Future deceleration, Statefinder diagnostics, Universe's age.

## 1 Introduction

Astronomical studies [1–3] have confirmed the expanding nature of the cosmos, which is an intriguing discovery of the observable universe. Afterwards, theoretical cosmologists became interested in creating cosmological models that depicted an accelerated phase of the universe's expansion. Multiple theoretical cosmologists have put forward models that either modify Einstein's field equations or suggest other theories of gravity in response to the universe's acceleration. A more appropriate cosmological models to explain the current growth in the universe's expansion has been proposed based on the dark energy. It is generally agreed that the dynamical cosmological term  $\Lambda$  is one of the most promising dark energy candidates [4]. However, there are multiple difficulties[4–6] with the  $\Lambda$  term model, including coincidence issues and fine tuning[6]. To deal with these present cosmological problems, various approaches have been proposed in the last few decades. Nowadays, the modified theory of gravity technique is the most often used option for resolving current cosmological issues. One of the most well-known ideas to the dark content problem of the universe is the  $f(R)$  gravity [7, 8] which

---

\*romanshugarg18@gmail.com

†tanmoych.ju@gmail.com

‡gpsingh@mth.vnit.ac.in

§rahaman@associates.iucaa.in

is a modification of General Relativity. With the evolving time, several other modified theories are also widely explored[9–33].

A relation between the Ricci scalar  $R$  with  $L_m$  denoting the matter Lagrangian density has given rise to the gravitational theory based on  $f(R, L_m)$  and is termed as the  $f(R, L_m)$  theory. Harko and Lobo [34] show that this theory provides a more general relation between matter and geometry sector. However, this approach violates the equivalence principle and the solar system observations impose stringent restrictions on these models [35–38]. This theory belong to the class of the most complete gravitational theories represented on Riemannian space [39, 40] and, offers novel perspectives on the intricate relationships between the geometries of cosmology-astrophysics and matter. Due to the presence of matter, the field equations of  $f(R, L_m)$  gravity and the  $f(R)$  model differ from each other and GR, but they coincides in empty space [34, 41]. In connection with the  $f(R, L_m)$  gravity, numerous further studies have been completed [42–51].

In the present paper, we probe the dynamics of dynamical dark energy in late universe of  $f(R, L_m)$  gravity with the parametrized EoS parameters. The considered EoS parameter of dark energy varies inversely with the redshift with form  $\omega = \frac{w_o}{z+1}$ . In another case, it possess exponential form given by  $\omega = \frac{w_o}{z+1} \exp\left(\frac{z}{z+1}\right)$ . These parametrization of dark energy are also termed as the Gong-Zhang parametrization [52–54]. There is only one parameter in these dark energy EoS parameters and, the dark energy does not diverge in the cosmological history according to these parameters. This well-behaved nature of dark energy in these parametrization makes them appropriate to model the deceleration-acceleration cosmic history. Further, the parameter  $w_o$  enables us to trace the present day EoS parameter. The cosmic history described by these parameters further enable us to describe the compatibility of expansion rate of the  $f(R, L_m)$  theory. The cosmological features may further be scrutinized based on the observational data. We investigate these EoS parameters in the outline of the  $f(R, L_m)$  cosmological model.

This work has been divided into seven sections: In Sec. (2), an overview of the  $f(R, L_m)$  gravity theory is briefly discussed. The field equations for the FLRW metric in  $f(R, L_m)$  gravity are presented in Sec. (3). In Sec. (4), the Hubble parameters in terms of red-shift using dark energy EoS parameters are derived. These parameters enable to provide the observational compatibility in Sec. (5). In particular, we derive the median values of model parameters by using the Bayesian analysis technique for Cosmic Chronometer (CC) data and a combined data set composed of CC and supernovae Type Ia observations. The physical and geometrical analysis based on the deceleration parameter and the physical parameters such as (pressure and energy density) are studied in Sec. (6). Furthermore, the statefinder diagnostic is used to examine the nature of dark energy based on the geometrical parameters. The universe age in these models are computed to describe the compatibility with Planck based results of  $\Lambda$ CDM model. The conclusions are given in the last section (7).

## 2 An Overview of $f(R, L_m)$ gravity theory

In this section, we discuss a overview of  $f(R, L_m)$  gravity and the action in  $f(R, L_m)$  gravity takes the form [34].

$$S = \int f(R, L_m) \sqrt{-g} d^4x, \quad (1)$$

where,  $L_m$  defines as matter-Lagrangian density and  $R$  refers to Ricci scalar. We can define Ricci scalar ( $R$ ) by using the Ricci tensor ( $R_{\mu\nu}$ ) with metric tensor ( $g^{\mu\nu}$ ) as

$$R = g^{\mu\nu} R_{\mu\nu}, \quad (2)$$

where the  $R_{\mu\nu}$  is

$$R_{\mu\nu} = \partial_c \Gamma_{\mu\nu}^c - \partial_\mu \Gamma_{cv}^c + \Gamma_{\mu\nu}^c \Gamma_{dc}^d - \Gamma_{vd}^c \Gamma_{\mu c}^d, \quad (3)$$

and  $\Gamma_{\beta\gamma}^\alpha$  signifies the Levi-Civita connection given by

$$\Gamma_{\beta\gamma}^\alpha = \frac{1}{2}g^{\alpha c} \left( \frac{\partial g_{\gamma c}}{\partial x^\beta} + \frac{\partial g_{c\beta}}{\partial x^\gamma} - \frac{\partial g_{\beta\gamma}}{\partial x^c} \right). \quad (4)$$

Using the action (1) with the metric tensor  $g_{\mu\nu}$ , the field equation may be written as,

$$\frac{\partial f}{\partial R} R_{\mu\nu} + (g_{\mu\nu} \square - \nabla_\mu \nabla_\nu) \frac{\partial f}{\partial R} - \frac{1}{2} \left( f - \frac{\partial f}{\partial L_m} L_m \right) g_{\mu\nu} = \frac{1}{2} \left( \frac{\partial f}{\partial L_m} \right) T_{\mu\nu}, \quad (5)$$

where  $T_{\mu\nu}$  is defined as the energy-momentum tensor for perfect fluid as

$$T_{\mu\nu} = \frac{-2}{\sqrt{-g}} \frac{\delta(\sqrt{-g}L_m)}{\delta g^{\mu\nu}}. \quad (6)$$

Using these field equations, we can construct a relationship between the Ricci scalar( $R$ ), the trace of the energy-momentum tensor  $T$  and the matter Lagrangian density ( $L_m$ ) as

$$R \left( \frac{\partial f}{\partial R} \right) + 2 \left( \frac{\partial f}{\partial L_m} L_m - f \right) + 3 \square \frac{\partial f}{\partial R} = \frac{1}{2} \left( \frac{\partial f}{\partial L_m} \right) T, \quad (7)$$

where the  $\square I = \frac{1}{\sqrt{-g}} \partial_\mu (\sqrt{-g} g^{\mu\nu} \partial_\nu I)$  for any type of random function  $I$ . To analyse the Eq. (5), we can substitute the covariant derivative with energy-momentum tensor, written as:

$$\nabla^\mu T_{\mu\nu} = 2 \nabla^\mu \log[f_{L_m}(R, L_m)] \frac{\partial L_m}{\partial g^{\mu\nu}}. \quad (8)$$

In the next section, we write the equations of motions in the FLRW spacetime.

### 3 Motion equations in $f(R, L_m)$ gravity

The observable universe is homogeneous and isotropic to a great extent. In order to describe this nature of universe, we employ the flat Friedman–Lemaître–Robertson–Walker (FLRW) metric [55] as:

$$ds^2 = a^2(t) (dx^2 + dy^2 + dz^2) - dt^2, \quad (9)$$

where at a given time  $t$ , the scale factor describing the cosmic evolution is denoted by  $a(t)$ . For the line element (9), the non-vanishing components of the Christoffel symbols are:

$$\Gamma_{pq}^0 = -\frac{1}{2}g^{00} \frac{\partial g_{pq}}{\partial x^0}, \quad \Gamma_{0q}^r = \Gamma_{q0}^r = \frac{1}{2}g^{r\lambda} \frac{\partial g_{q\lambda}}{\partial x^0}, \quad (10)$$

where the variables  $p, q, r = 1, 2, 3$ . By utilizing equation (3), the non-vanishing components of the Ricci tensor and, the Ricci scalar are written as:

$$R_0^0 = 3 \frac{\ddot{a}}{a}, \quad R_1^1 = R_2^2 = R_3^3 = \frac{\ddot{a}}{a} + 2 \left( \frac{\dot{a}}{a} \right)^2, \quad R = 6 \left( \frac{\dot{a}}{a} \right)^2 + 6 \left( \frac{\ddot{a}}{a} \right) = 12H^2 + 6\dot{H}, \quad (11)$$

where  $H = \frac{\dot{a}}{a}$  denotes the Hubble parameter describing the expansion rate. For the perfect fluid, we take the energy-momentum tensor as

$$T_{\mu\nu} = (p + \rho)u_\mu u_\nu + pg_{\mu\nu}, \quad (12)$$

where  $p$  and  $\rho$  are defined as the isotropic pressure and the energy density of the cosmic fluid and the components of the four velocity are  $u^\mu = (1, 0, 0, 0)$  satisfying  $u_\mu u^\mu = -1$ . The Friedmann equations that describe the dynamics relation of the universe in  $f(R, L_m)$  gravity can be read as follows:

$$\frac{1}{2}(f - f_{L_m}L_m - f_R R) + 3H\dot{f}_R + 3H^2 f_R = \frac{1}{2}f_{L_m}\rho, \quad (13)$$

$$3H^2 f_R + \dot{H}f_R - \ddot{f}_R - 3H\dot{f}_R + \frac{1}{2}(-f + f_{L_m}L_m) = \frac{1}{2}f_{L_m}p. \quad (14)$$

These field equations are useful to derive the expansion rate expression for the description of cosmological history and the transiting universe evolution.

## 4 The expansion rate and background dynamics in the $f(R, L_m)$ model

In this section, we choose a specific form of  $f(R, L_m)$  gravity [56] described by:

$$f(R, L_m) = \frac{R}{2} + L_m^\alpha, \quad (15)$$

where  $\alpha$  is an arbitrary constant. For this specified functional form of the  $f(R, L_m)$  model with  $L_m = \rho$  [57], equations (13) and (14) would become

$$3H^2 = (2\alpha - 1)\rho^\alpha, \quad (16)$$

$$2\dot{H} + 3H^2 = (\alpha - 1)\rho^\alpha - \alpha p\rho^{\alpha-1}. \quad (17)$$

Mathematically, the Equation of State (EoS) parameter is given by  $\omega = \frac{p}{\rho}$ . We use equations (16), (17) and  $\dot{H} = -H(1+z)\frac{dH}{dz}$  to write the EoS parameter  $\omega$  as

$$\omega = \frac{2(2\alpha - 1)(z+1)H' - 3\alpha H}{3\alpha H}. \quad (18)$$

Here, we have two independent equations (16) and (17) with three unknown parameters,  $a(t)$ ,  $\rho$  and  $p$ . To derive a specified solution, we may need an additional equation to solve equation (18). We utilize the reciprocal- and exponential-like EoS parameters [52] to solve equation (18). Thereafter, now the number of unknowns and the number of equations are same.

### 4.1 Model-I

In this model, we investigate with reciprocal-like equation of state parameter [52],

$$\omega = \frac{w_0}{z+1}, \quad (19)$$

where, we may use the observations to constrain the parameter  $w_0$ . In the outline of cosmological modelling, this EoS parameter offers several important advantages. First of all, it offers a framework that can be physically understood with parameter  $w_0$ . This parameter is denoting the DE EoS parameter at the current epoch ( $z = 0$ ). The inclusion of red-shift dependency enables to characterize the evolution of DE. As  $z$  goes more rapidly towards infinity (in the past),  $\omega \sim 0$ , which demonstrates that the DE EoS parameter leans towards zero at early era. As  $z \rightarrow -1$  (in the asymptotic limit),  $\omega \rightarrow -\infty$ , it indicates that the DE EoS parameter leans towards negative infinity

in the far future. These properties of the DE EoS parameter are reasonable and attractive alternative to study its evolution in  $f(R, L_m)$  gravity. From equation (18) and (19), we get

$$\frac{w_o}{z+1} = \frac{2(2\alpha-1)(z+1)H' - 3\alpha H}{3\alpha H}. \quad (20)$$

By solving equation (20), we obtain the Hubble parameter's expression as follows

$$H(z) = H_0 \exp \left( \frac{3\alpha(zw_o + (z+1)\log(z+1))}{2(2\alpha-1)(z+1)} \right). \quad (21)$$

where  $H_0$  denotes the current value of the Hubble parameter. In the  $f(R, L_m)$  gravity, the reciprocal-like EoS parameter yields the Hubble parameter with exponential function and leads to a non-trivial evolution as compared to the  $\Lambda$ CDM model. It would be interesting to investigate whether this model traces the matter-dominated era of the universe evolution or not.

## 4.2 Model-II

In this model, we investigate with exponential-like equation of state parameter [52] as

$$\omega = \frac{w_o}{z+1} \exp \left( \frac{z}{z+1} \right) \quad (22)$$

When  $z \gg 1$ ,  $\omega \sim 0$ . A significant distinction between model (19) and model (22) is that in model (22),  $\omega$  approaches 0 when  $z \rightarrow -1$ . In the past, these two forms exhibited nearly identical behavior but their future evolution diverges significantly. From equations (18), (22) and after solving them, we obtain the Hubble parameter with respect to redshift as,

$$H(z) = H_0 \exp \left[ \frac{3\alpha \left( \log(1+z) + (-1 + \exp(-\frac{z}{1+z})) w_0 \right)}{4\alpha - 2} \right] \quad (23)$$

where  $H_0$  defined as Hubble parameter value at  $z = 0$ .

## 5 Observational constraints

In this section, we test the observational compatibility of the expansion rates (21) and (23) by conducting a Bayesian analysis with the observations of cosmic chronometer and supernovae type Ia (Pantheon) sample. We employ the joint data sample and term it as the CC+Pantheon sample. The Bayesian analysis is employed to conduct the  $\chi^2$  minimization with the Markov Chain Monte Carlo (MCMC) technique. We use the emcee Python library [58] in the present analysis.

### 5.1 The observation of Cosmic chronometer dataset

We analyse the CC data set with 31 observations. The observations are acquired via the differential ages (DA) method of passively evolving galaxies and the range of redshift is  $0.07 \leq z \leq 1.965$ . This investigation focuses on determining the median values of the model parameters. According to the basic principle set up by Jimenez and Loeb[59], the relationship between the Hubble parameter ( $H(z)$ ), cosmic-time ( $t$ ), and redshift ( $z$ ) may be

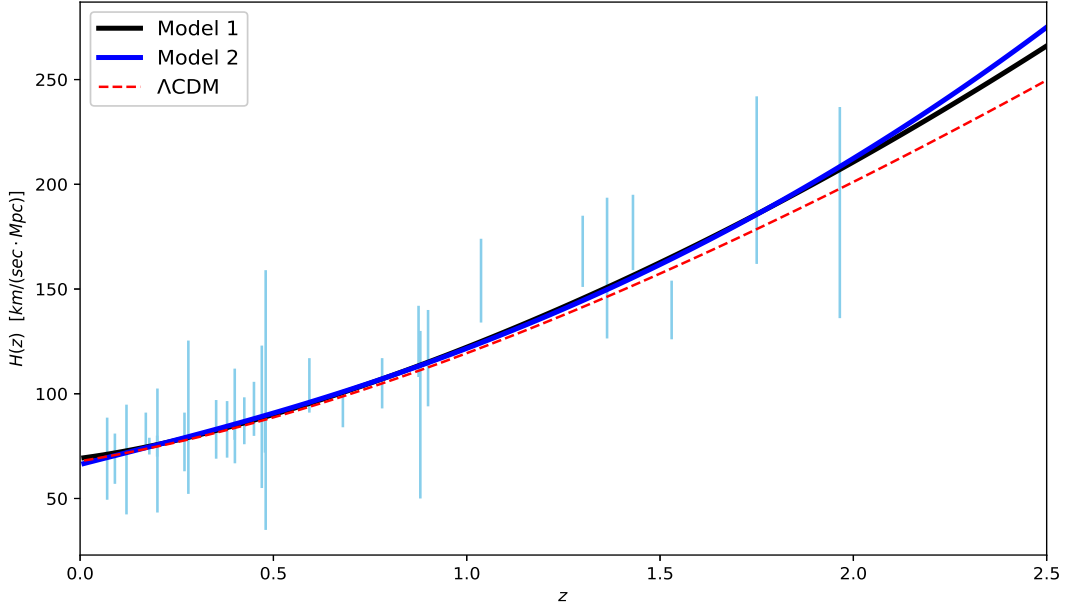


Figure 1: In comparison to the  $\Lambda$ CDM model, the best fit Hubble parameters (given by Eq. (21) and (23)) with  $z$ .

stated as follows:  $H(z) = \frac{-1}{(1+z)} \frac{dz}{dt}$ . We determine the model parameters  $H_0, w_0$  and  $\alpha$  through the minimization of the  $\chi^2$  function (which is comparable to the maximizing likelihood function) expressed as [60–62].

$$\chi_{CC}^2(\theta) = \sum_{i=1}^{i=31} \frac{[H_{th}(\theta, z_i) - H_{obs}(z_i)]^2}{\sigma_{H(z_i)}^2}. \quad (24)$$

Here,  $H_{th}$  characterizes the theoretical value of Hubble parameter,  $H_{obs}$  characterizes its observed value and  $\sigma_H$  characterizes the standard error of the observed value. The error between the CC data points and the best-fit Hubble parameter curve is displayed in figure (1). Furthermore, figure (2) and (3) represent a contour map demonstrating the  $1\sigma$  and  $2\sigma$  likelihood confidence levels for the median values of  $H_0, w_0$  and  $\alpha$  obtained from the CC data.

## 5.2 The observation of Pantheon dataset

We also utilize the Pantheon dataset, which comprising 1048 Type Ia supernovae data points for the redshift range  $0.01 < z < 2.26$  [63]. The SNIa sample is composed of the data from surveys such as CfA1-CfA4 [64, 65], Pan-STARRS1 Medium Deep Survey [63], SDSS [66], SNLS [67], and the Carnegie Supernova Project (CSP) [68]. The theoretically expected apparent magnitude  $\mu_{th}(z)$  is determined by

$$\mu_{th}(z) = M + 5 \log_{10} \left[ \frac{d_L(z)}{Mpc} \right] + 25, \quad (25)$$

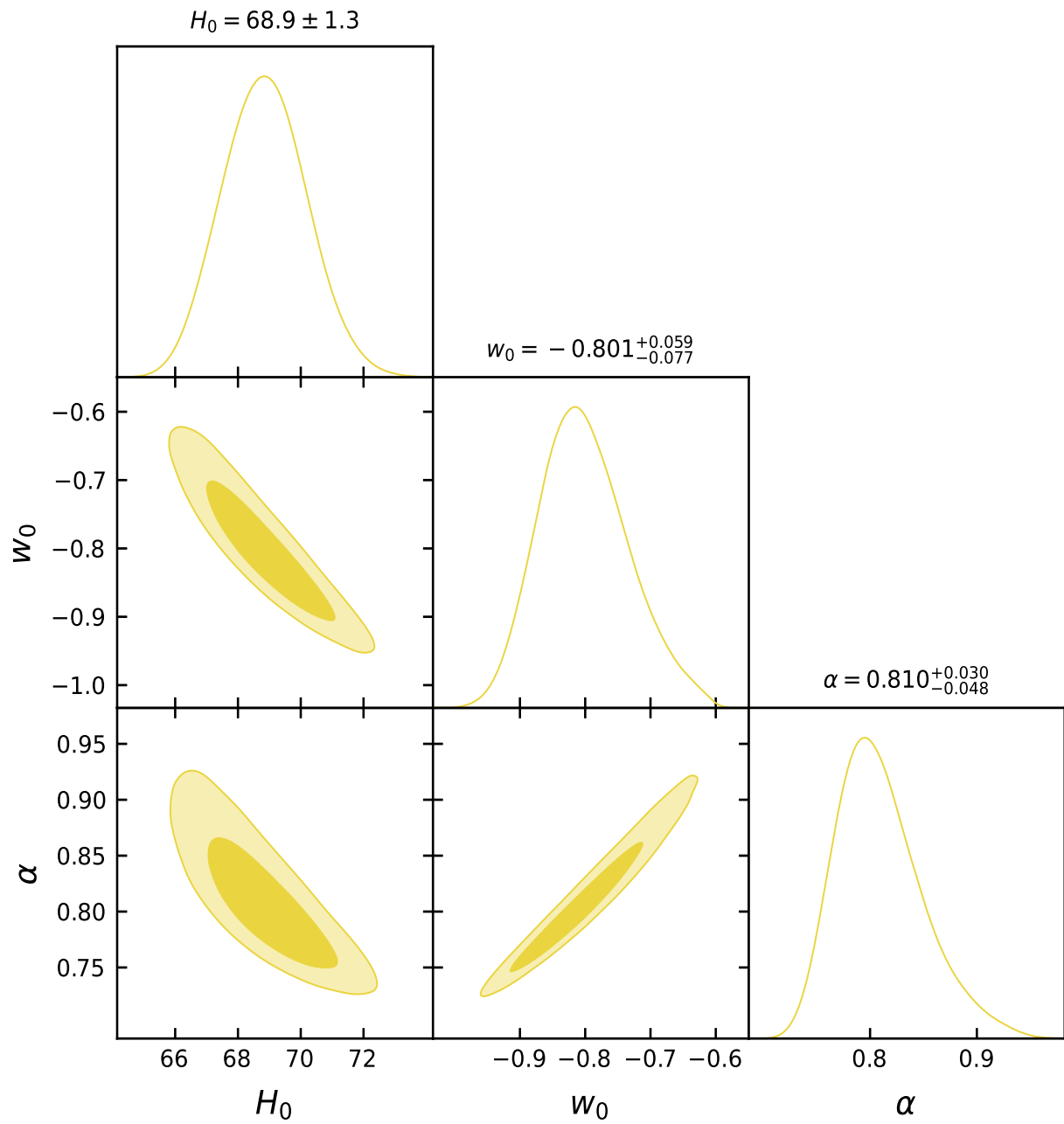


Figure 2: Model-I: Marginalized  $1\sigma$  and  $2\sigma$  contours map with median values of  $H_0$ ,  $w_0$  and  $\alpha$  for CC data set.

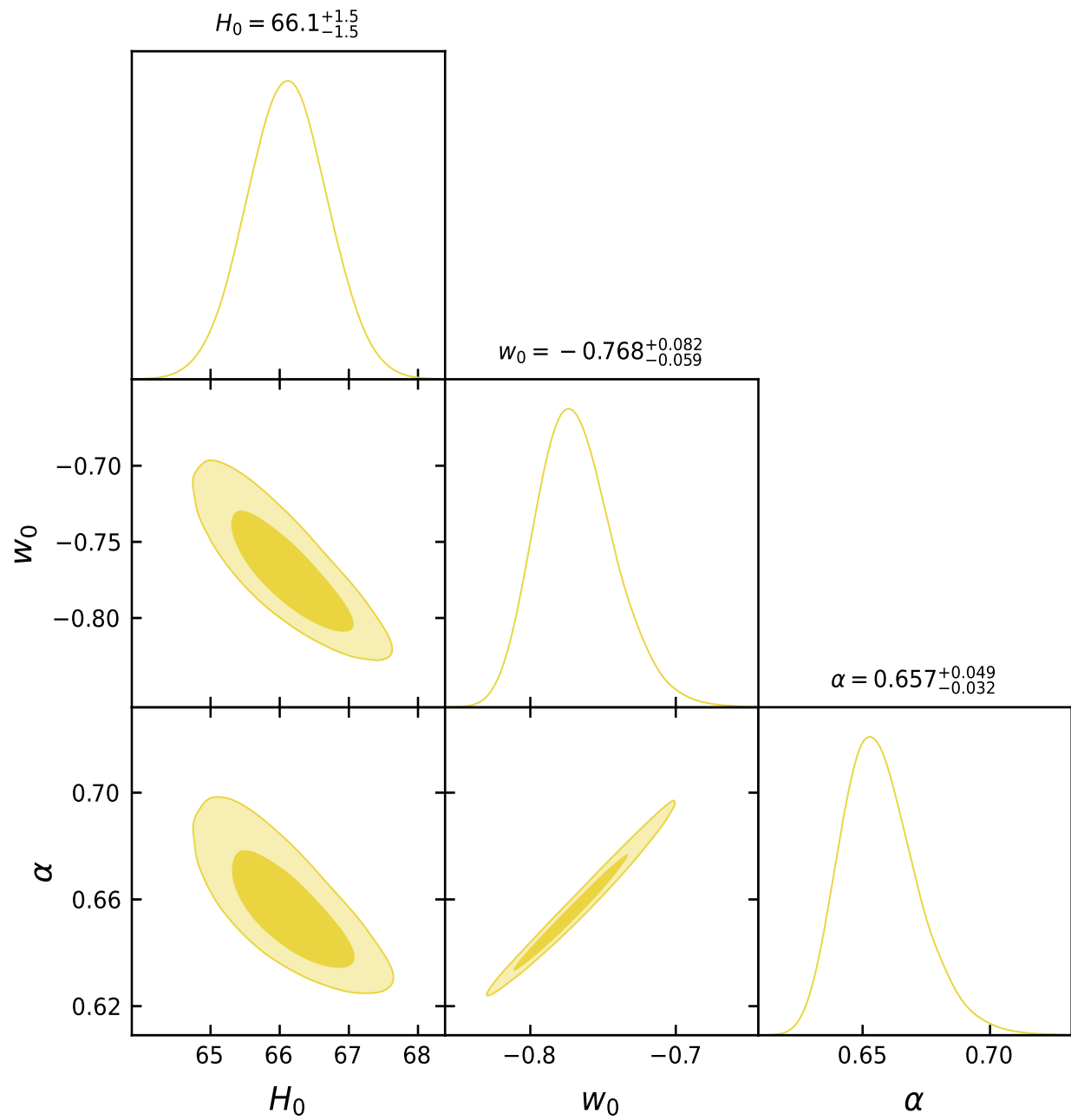


Figure 3: Model-II: Marginalized  $1\sigma$  and  $2\sigma$  contours map with median values of  $H_0$ ,  $w_0$  and  $\alpha$  for CC data set.

where  $M$  is the absolute magnitude. Also, the luminosity distance  $d_L(z)$  (having dimension of the Length) may be written as [69]

$$d_L(z) = c(1+z) \int_0^z \frac{dz'}{H(z')}, \quad (26)$$

where the parameter  $z$  signifies SNIa's redshift as determined in the cosmic microwave background (CMB) rest frame and  $c$  is defined as speed of the light. The luminosity distance ( $d_L$ ) is often replaced by the dimensionless Hubble-free luminosity distance ( $D_L(z) \equiv H_0 d_L(z)/c$ ). Equation (25) can be written in the following way

$$\mu_{th}(z) = M + 5 \log_{10} [D_L(z)] + 5 \log_{10} \left[ \frac{c/H_0}{Mpc} \right] + 25. \quad (27)$$

There will be a degeneracy between  $H_0$  and  $M$  in the  $\Lambda$ CDM model framework [70, 71]. We express  $\mathcal{M}$  as a combination of these parameters as shown below.

$$\mathcal{M} \equiv M + 5 \log_{10} \left[ \frac{c/H_0}{Mpc} \right] + 25 = M - 5 \log_{10}(h) + 42.38, \quad (28)$$

where  $H_0 = h \times 100 \frac{Km}{s.(Mpc)}$ . In MCMC analysis, we employ these parameter with appropriate  $\chi^2$  for the Pantheon dataset as [25, 60, 62, 71, 72]

$$\chi_P^2 = \nabla \mu_i C_{ij}^{-1} \nabla \mu_j, \quad (29)$$

whereas  $\nabla \mu_i = \mu_{obs}(z_i) - \mu_{th}(z_i)$ ,  $C_{ij}^{-1}$  defined as the inverse of covariance matrix and  $\mu_{th}$  may be specified by equation (27).

The luminosity distance is contingent on the Hubble parameter. Following this approach, we utilize the emcee package [58] and equations (21), (23) to obtain the maximum likelihood estimate (MLE) by using the combined of CC+Pantheon data set. We define the joint  $\chi^2$  expression as  $\chi_{total}^2 = \chi_{CC}^2 + \chi_P^2$  for computing the maximum likelihood estimate using the joint data. Figure (4) and (5) is exhibited for  $1\sigma$  and  $2\sigma$  likelihood contour maps and 1D distributions with MCMC analysis through combined of CC+Pantheon datasets.

For Model I (21) and Model II (23), the median values of the model parameters computed through MCMC analysis with emcee are provided in tables (1) and (2).

Dataset	$H_0$ [Km/(s.Mpc)]	$w_0$	$\alpha$	$\mathcal{M}$	$q_0$	$z_t$	$t_0$ [Gyr]
CC	$68.9^{+1.3}_{-1.3}$	$-0.801^{+0.059}_{-0.077}$	$0.810^{+0.030}_{-0.048}$	-	-0.60	0.635	$13.22^{+0.165}_{-0.34}$
CC+Pantheon	$69.1^{+1.9}_{-1.9}$	$-0.779^{+0.059}_{-0.059}$	$0.843^{+0.053}_{-0.084}$	$23.807^{+0.013}_{-0.013}$	-0.59	0.71	$13.41^{+0.14}_{-0.46}$

Table 1: **Model-I:** Median values of model parameters with the current values of  $q_0$ ,  $z_t$  and  $t_0$  for CC and joint data sets.

Dataset	$H_0$ [Km/(s.Mpc)]	$w_0$	$\alpha$	$\mathcal{M}$	$q_0$	$z_t$	$t_0$ [Gyr]
CC	$66.1^{+1.5}_{-1.5}$	$-0.768^{+0.082}_{-0.059}$	$0.657^{+0.049}_{-0.032}$	-	-0.2718	0.7	$12.74^{+0.18}_{-0.14}$
CC+Pantheon	$68.9^{+1.9}_{-1.9}$	$-0.822^{+0.015}_{-0.055}$	$0.6452^{+0.0088}_{-0.045}$	$23.824^{+0.011}_{-0.011}$	-0.4067	0.871	$12.62^{+0.33}_{-0.22}$

Table 2: **Model-II:** Median values of model parameters with the current values of  $q_0$ ,  $z_t$  and  $t_0$  for CC and joint data sets.

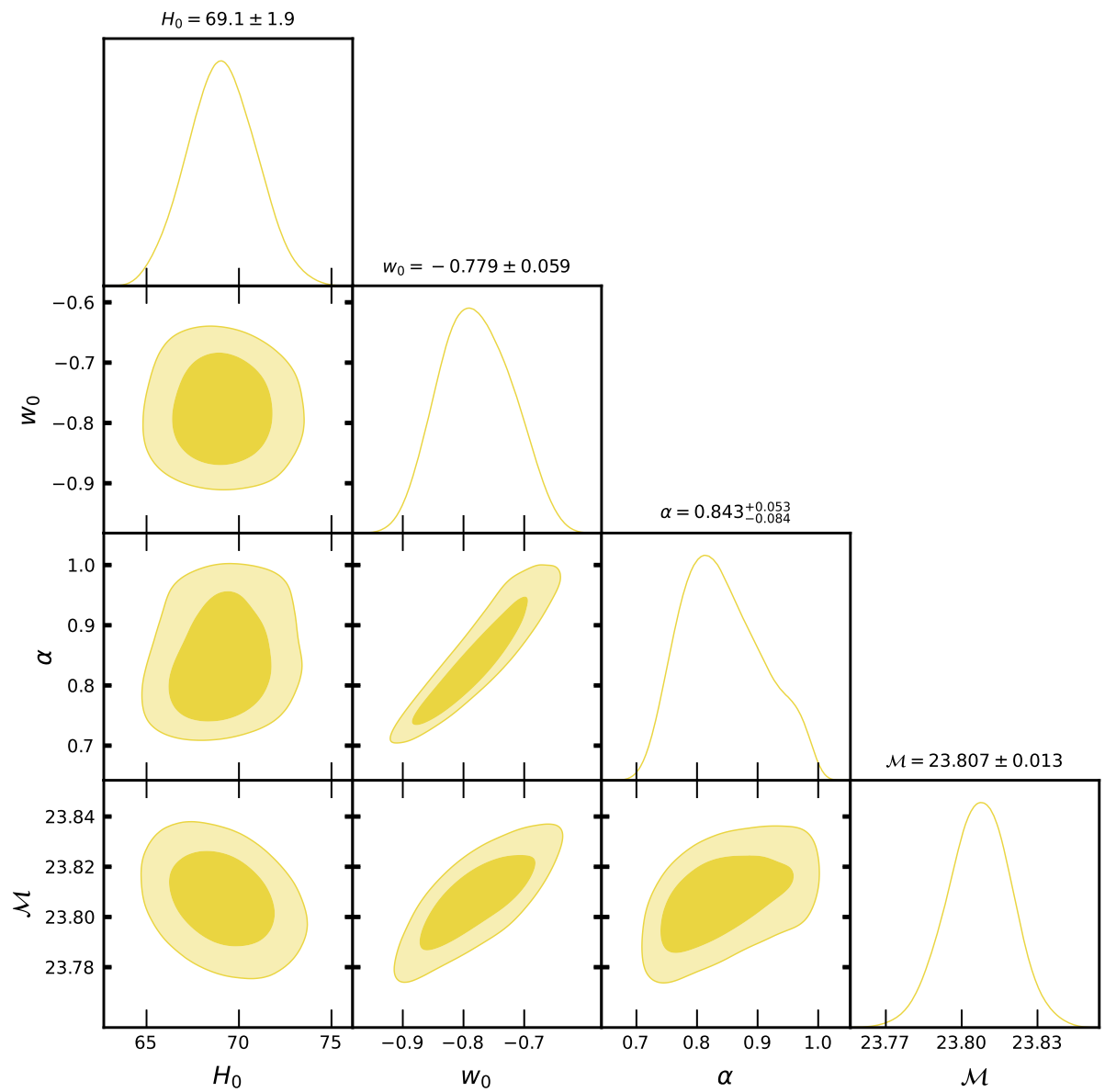


Figure 4: Model-I: 1 $\sigma$  and 2 $\sigma$  likelihood contours map for the Joint dataset.

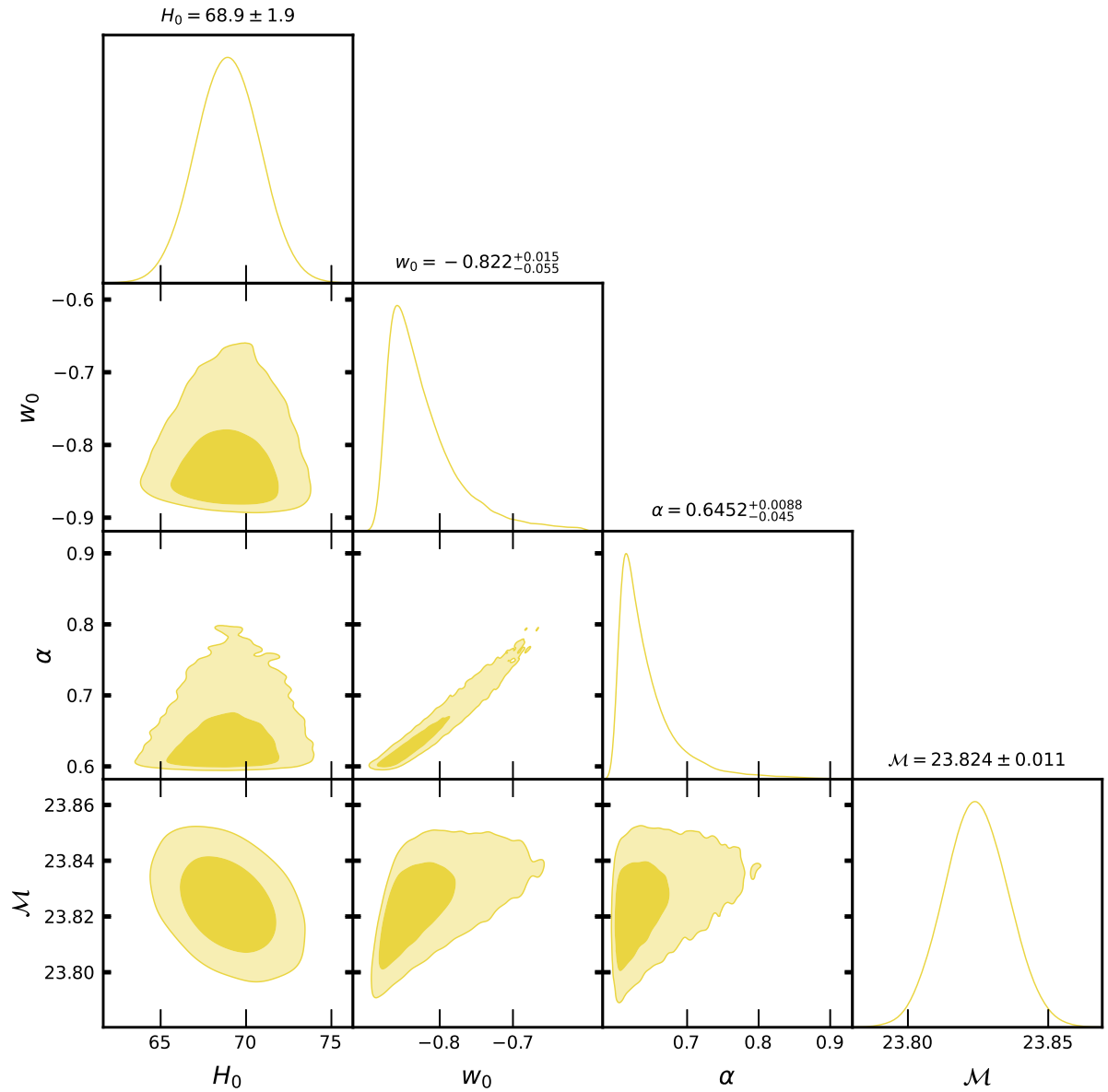


Figure 5: Model-II: 1 $\sigma$  and 2 $\sigma$  likelihood contours map for the Joint dataset.

## 6 The physical and dynamical characteristics

### 6.1 Analysis of Deceleration parameter

The deceleration parameter ( $q$ ) plays a crucial role in describing the expansion behaviour of the universe. Variations values of the deceleration parameter ( $q$ ) are used to illustrate the different phases of universe's expansion. The universe expands with acceleration for  $q < 0$  and it decelerate for  $q > 0$ . When the deceleration parameter is smaller than  $-1$ , the cosmos enters a period of super accelerated expansion. The de Sitter, matter-dominated and radiation-dominated phases of the universe are for  $-1$ ,  $\frac{1}{2}$  and  $1$  respectively. The deceleration parameter may be expressed as

$$q = -1 + \frac{d}{dt} \frac{1}{H}. \quad (30)$$

By using (21), (23) and (30), we obtain for Model I and II as,

$$q(z) = \frac{3\alpha w_0 - (\alpha - 2)(z + 1)}{2(2\alpha - 1)(z + 1)}, \quad (31)$$

$$q(z) = \frac{-(\alpha - 2)(1 + z) + 3\alpha w_0 \exp\left(\frac{z}{1+z}\right)}{2(1 + z)(2\alpha - 1)}, \quad (32)$$

respectively. The analysis of deceleration parameters for Model I and Model II are presented in figures (6) and (7). For model I, figure (6) demonstrates the transition of the universe's evolution from a decelerated expansion phase to an accelerated expansion phase. This transition occurs at  $z = 0.635$  and  $z = 0.71$  with median values for CC data and joint data set respectively. For Model I the current values of deceleration parameter are  $q_0 = -0.6$  (for CC data) and  $q_0 = -0.59$  (for joint data). The negative value signifies that the universe is currently undergoing accelerated expansion. It is evident from the analysis that the deceleration parameter is consistent with present accelerated expansion phase.

According to figure (7), in Model II, the present value of deceleration parameter is  $q_0 = -0.2718$  for the CC estimate and  $q_0 = -0.4067$  for the Joint estimate. The universe transitions from a decelerated to an accelerated expansion phase at  $z = 0.7$  and  $z = 0.871$  for CC and joint data respectively. For red-shift  $z < 0.7$ , the accelerated phase of cosmic expansion can be observed in Model II. The model explains the accelerated expansion era in the present time, which is consistent with observations. Decelerated expansion phase is predicted by the model in future, which may be possibly due to the energy exchange between dark matter and dark energy. In this scenario, energy is transferred from dark energy to dark matter. Several studies in the literature which predict this type of behavior in the future[54, 73, 74].

### 6.2 The energy density, pressure and equation of state parameter

We study the physical characteristics demonstrated by key quantities such as the energy density and pressure. For the constrained parameters, the energy density is still positive during the cosmic expansion, although the pressure might become negative. For the accelerated expansion of the universe, energy density has been consistently positive while pressure demonstrates negative behavior in the present time and future. Using the equations (16), (21) and (23), energy density in these models may be written as:

$$\rho(z) = \left(\frac{3}{2\alpha - 1}\right)^{1/\alpha} \left(H_0^2 \exp\left(\frac{3\alpha \left(\log(z+1) + \frac{zw_0}{z+1}\right)}{2\alpha - 1}\right)\right)^{1/\alpha} \quad (Model - I) \quad (33)$$

$$\rho(z) = \left(\frac{3}{2\alpha - 1}\right)^{1/\alpha} \left(H_0^2 \exp\left[\frac{6\alpha \left(\log(1+z) + (-1 + \exp\left(\frac{z}{1+z}\right)) w_0\right)}{4\alpha - 2}\right]\right)^{1/\alpha} \quad (Model - II) \quad (34)$$

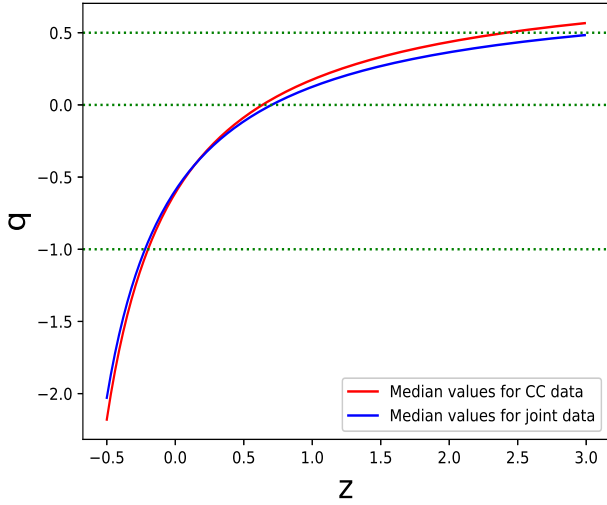


Figure 6: **For Model-I:**  $q$  with  $z$ .

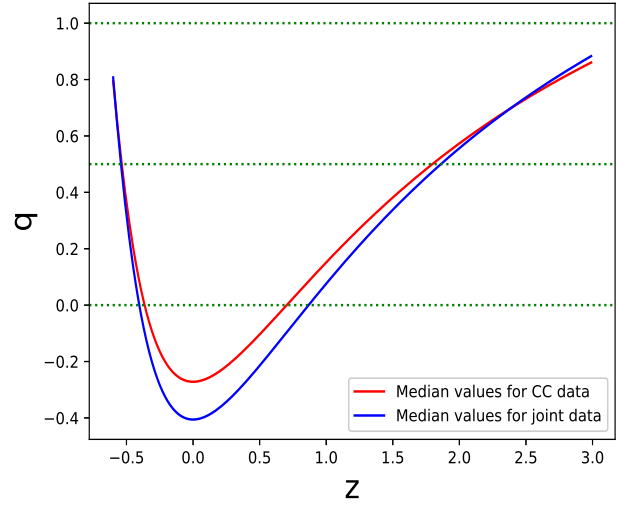


Figure 7: **For Model-II:**  $q$  with  $z$ .

From using equations (17), (21), and (23), pressure for Model-I and Model-II can be written as:

$$p(z) = \left[ \frac{w_0}{z+1} \right] \left( \frac{3}{2\alpha-1} \right)^{1/\alpha} \left( H_0^2 \exp \left( \frac{3\alpha(\log(z+1) + \frac{z \cdot w_0}{z+1})}{2\alpha-1} \right) \right)^{1/\alpha} \quad (\text{Model - I}) \quad (35)$$

$$p(z) = \left[ \frac{w_0}{z+1} \exp \left( \frac{z}{z+1} \right) \right] \left( \frac{3}{2\alpha-1} \right)^{1/\alpha} \left( H_0^2 \exp \left[ \frac{6\alpha(\log(1+z) + (-1 + \exp(\frac{z}{1+z})) w_0)}{4\alpha-2} \right] \right)^{1/\alpha} \quad (\text{Model - II}) \quad (36)$$

For the constrained parameters, the behavior of energy density as well as the pressure are shown in figure (8) (for model-I) and figure (9) (for model-II) respectively. These figures demonstrate that the energy densities will increase with red-shift ( $z$ ) (decrease with cosmic time ( $t$ )) and remains positive for both the models throughout during expansion. The energy density remains to be positive, supporting the ongoing expansion of the universe. In Model-I, pressure starts with positive values at high red-shift in the early universe while in both current and later epoch, Model-I exhibit negative pressure. These studies are consistent with the accelerating universe's expanding behavior.

The EoS parameter serves as a vital tool for identifying the nature of dark energy in the cosmological models. The relationship between pressure ( $p$ ) and energy density ( $\rho$ ) within the universe is described by the EoS parameter. Mathematically, it is defined as  $\omega = \frac{p}{\rho}$ . The dust phase ( $\omega = 0$ ), the radiation-dominated phase ( $\omega = \frac{1}{3}$ ), and the vacuum energy phase ( $\omega = -1$ ) corresponding with the  $\Lambda$ CDM model are some of the phases seen through the EoS parameter. Furthermore, there is the accelerated expansion period of the universe for ( $\omega < -\frac{1}{3}$ ).

Figures (10) and (11) illustrate the graphical evolution of the EoS parameter for the models. At present ( $z = 0$ ), the estimated values of the EoS parameter are  $\omega = -0.801$  for the CC dataset and  $\omega = -0.779$  for the joint dataset in Model I. In model II, the EoS parameter values are  $\omega = -0.768$  and  $\omega = -0.822$  at  $z = 0$  for CC and joint estimates data respectively.

These models possess a quintessence-like dark energy at the present epoch as shown by the behavior of the EoS

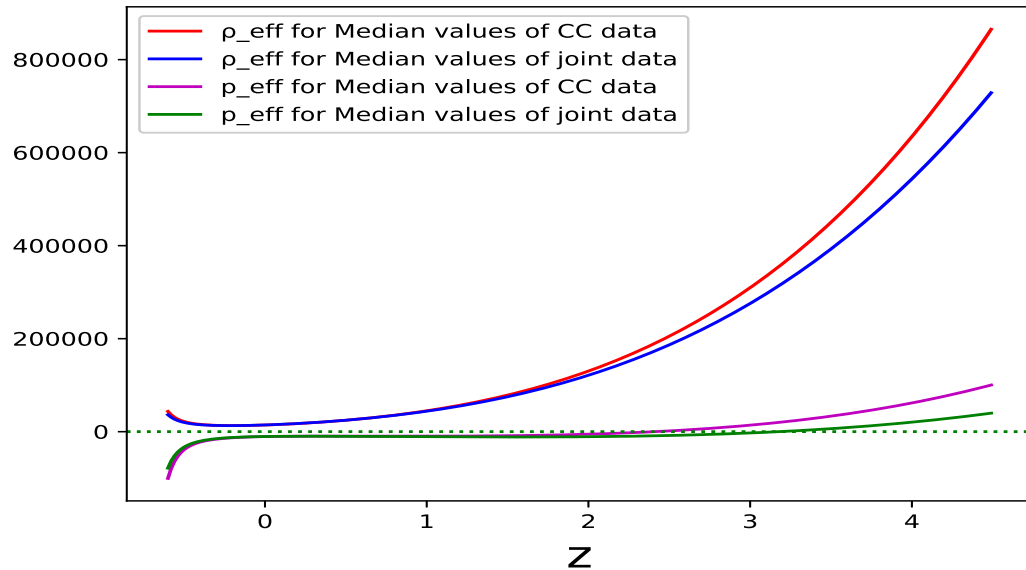


Figure 8: **For Model-I:**  $\rho_{eff}$  and  $p_{eff}$  with  $z$

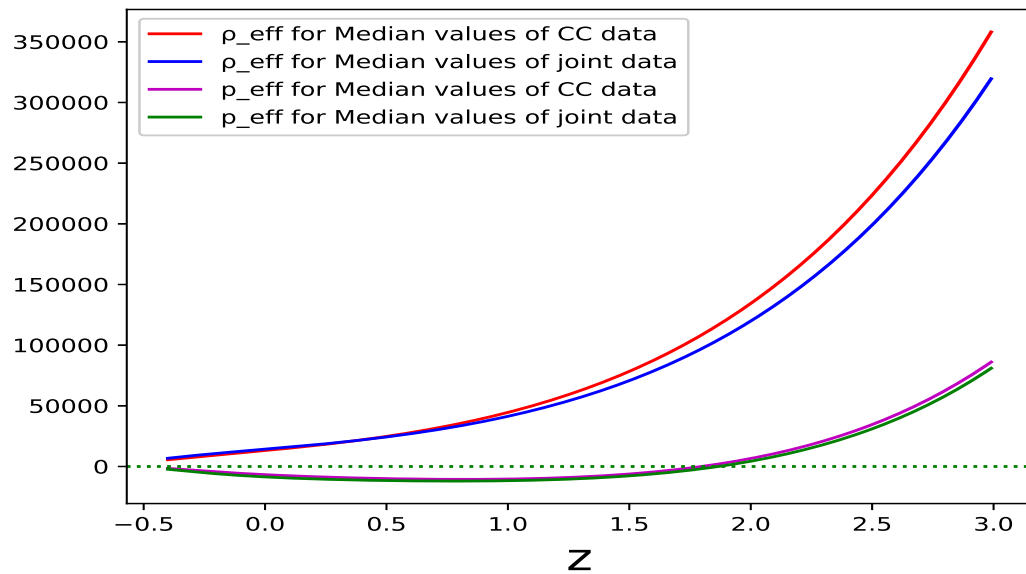


Figure 9: **For Model-II:**  $\rho_{eff}$  and  $p_{eff}$  with  $z$

parameter's figures (10) and (11). In Model I,  $\omega$  will eventually cross the  $\omega = -1$  line, having phantom dark energy dominated behavior in future. The dynamics of Model II indicate a possible energy exchange between dark matter and dark energy, potentially causing future deceleration era in this model. This feature of the model stands out as particularly intriguing.

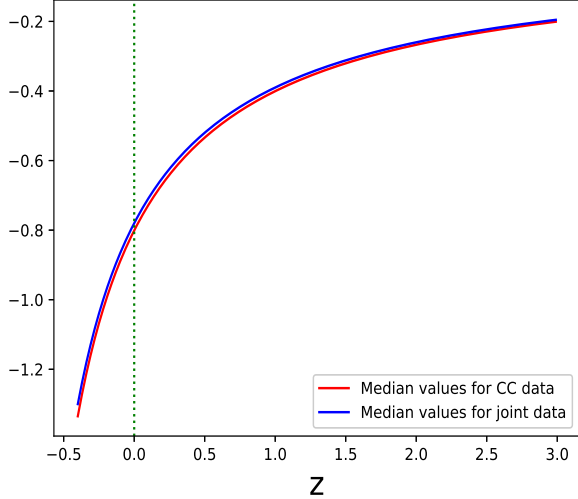


Figure 10: **For Model I:**  $\omega$  with  $z$ .

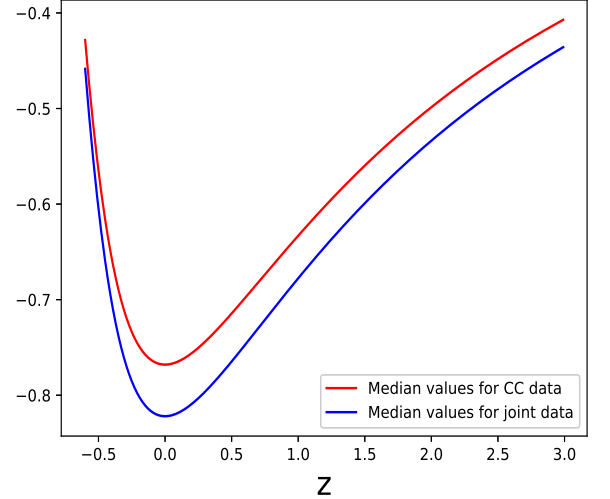


Figure 11: **For Model II**  $\omega$  with  $z$ .

### 6.3 Energy conditions

At a specific point in space-time, the point-wise energy conditions that rely solely on the stress energy tensor are as follows [30, 31, 75]:

NEC:- Null Energy Condition ( $\rho_{eff} + p_{eff} \geq 0$ ) always demonstrates that the addition of energy density and pressure is positive.

WEC:- The condition of weak energy indicates that both of the energy density and the sum of pressure-energy density are non-negative. ( $\rho_{eff} \geq 0$ ,  $\rho_{eff} + p_{eff} \geq 0$ )

DEC:- Dominant energy condition is denoted by the positivity of energy density ( $\rho_{eff}$ ) and ( $\rho_{eff} \geq |p_{eff}|$ ).

SEC:- Strong energy condition is composed of the conditions  $\rho_{eff} + 3p_{eff} \geq 0$  and  $\rho_{eff} + p_{eff} \geq 0$ .

In the decelerating era, the gravitational mass ( $\rho_{eff} + 3p_{eff}$ ) continues to be positive. Nevertheless, observational evidence proposes a potential violation of this condition sometimes between the era of galaxy formation and the present time. This variation shows the possible presence of component having negative pressure, and it displays anti-gravitational properties. Meanwhile, the Strong Energy Condition (SEC) contains two inequalities. It is important to remember that the violation of either one will violate the SEC [31–33].

All energy conditions for Model-I are graphically illustrated in figures (12). From the graphical results in Fig. (12), it is evident that the Model-I satisfies NEC, WEC, and DEC upto present time. Because the reconstructed model shows current accelerated expansion, so the SEC (specifically  $\rho_{eff} + 3p_{eff} > 0$ ) is violated. As the Universe enters into phantom era during future, the NEC is violated, which may also lead to the violation of WEC and DEC. However, for the constrained values according to both data sets, the violation of  $(\rho_{eff} + p_{eff}) \geq 0$

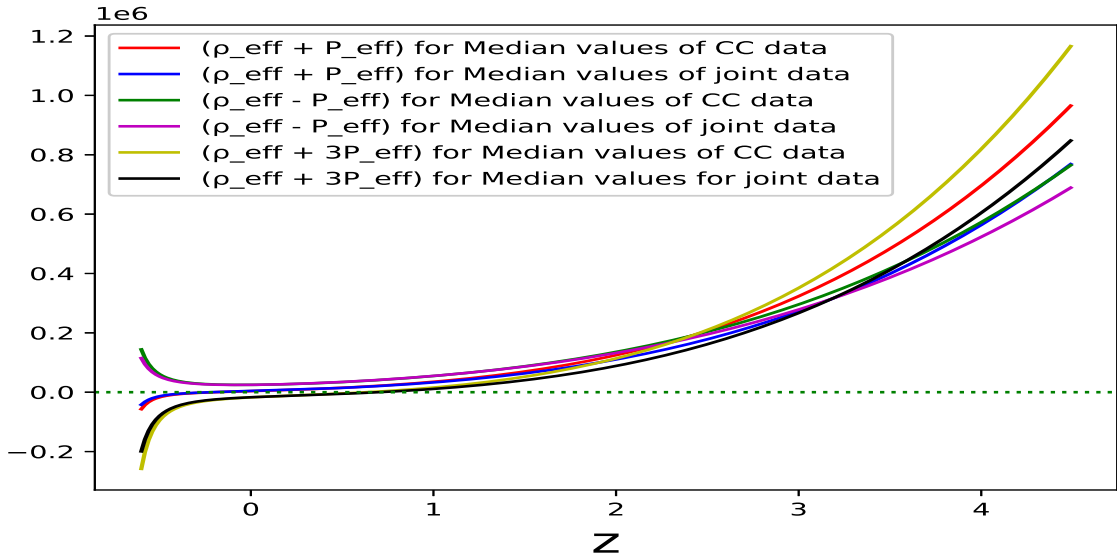


Figure 12: **For Model I:** The components of energy conditions with  $z$

points for the presence of phantom kind of dark energy in the model. We may conclude that the phantom kind of dark energy may not be ruled out in this model. In the phantom dark energy dominated era, the violation of  $\rho_{eff} + 3p_{eff} > 0$  will also be valid.

For Model-II, graphical representations of all energy conditions are illustrated in figure (13). It is observed that  $(\rho_{eff} + p_{eff}) > 0$ , and  $(\rho_{eff} - p_{eff}) > 0$  for the median values of model parameters. Further, the trajectory of  $(\rho_{eff} + 3p_{eff})$  transits from positive to negative values in present era.

#### 6.4 Statefinder diagnostic

It is broadly acknowledged that the geometric parameters of the cosmological model may offer the profound intuitions for its dynamical behaviour. To explore different dark energy models other than to the standard  $\Lambda$ CDM model, it becomes vital to analyse additional parameters other than the Hubble parameter and deceleration parameter. Higher-order derivatives of the scale factor  $a(t)$  occurs as essential tools to define the dynamical characteristics of the universe. It leads us to discuss about the geometric parameters, which are consisting the higher derivatives of scale factor ( $a$ ). Sahni et al. [76, 77] presented a pair of geometrical parameters, symbolized by  $(r, s)$  and termed as the *statefinder diagnostics*. The statefinder diagnostic is an effective tool for analyzing dark energy evolution in a model. The expressions for this diagnostic pair is given by:

$$r = \frac{\ddot{a}}{aH^3}, \quad s = \frac{r-1}{3(q-\frac{1}{2})}, \quad \text{where } q \neq \frac{1}{2}. \quad (37)$$

Various dark energy (DE) models discussed in the literature can be characterized by different values of the statefinder pair  $(r, s)$ :

- For Chaplygin gas (CG) model, one may have  $(r > 1, s < 0)$ .
- The  $\Lambda$ CDM model correspond to  $r = 1, s = 0$ .
- For Quintessence model, one may have  $(r < 1, s > 0)$ .

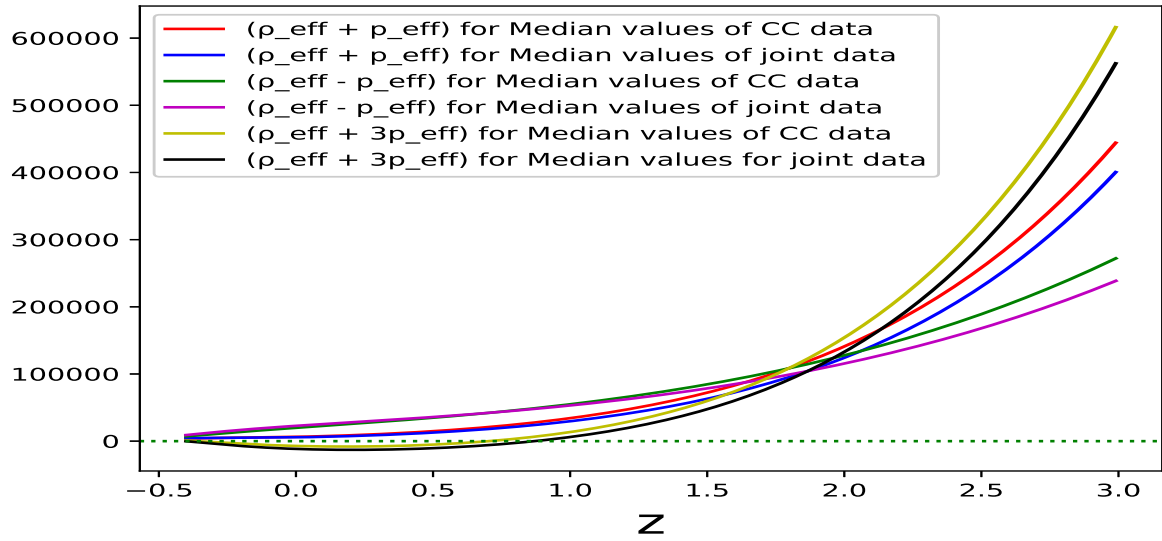


Figure 13: **For Model-II:** The components of energy conditions with  $z$

- For Holographic dark energy model (HDE),  $(r = 1, s = \frac{2}{3})$ .
- For Standard cold dark matter (SCDM), one may have  $(r = 1, s = 1)$ .

The figures (14) and (15) illustrate the  $(s, r)$  curve for Model I and Model II respectively. In figure (14), we see that for both data sets, the trajectory begins in the Chaplygin gas area during initial times, traverses the  $\Lambda$ CDM point and ultimately develops by unifying the dark matter and dark energy in the model.

Figure (15) illustrate that the evolution of the  $(s, r)$  parameters initially start Chaplygin gas models, passes through the  $\Lambda$ CDM point and finally evolve like quintessence models in the present epoch for both data estimates.

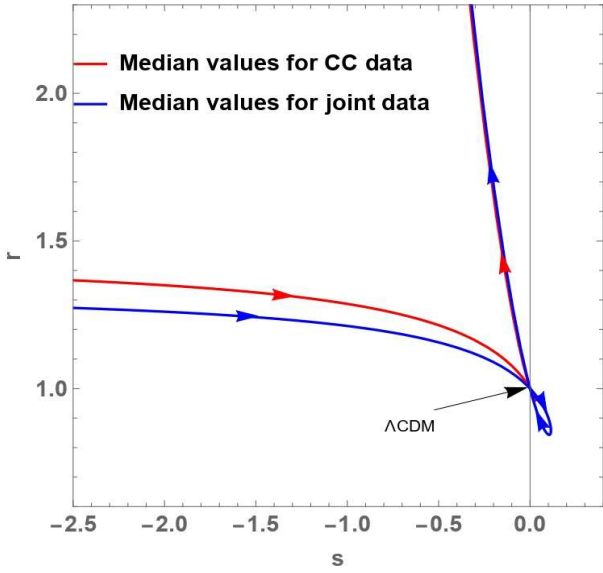


Figure 14: Model-I: Statefinder  $(r, s)$  trajectory.

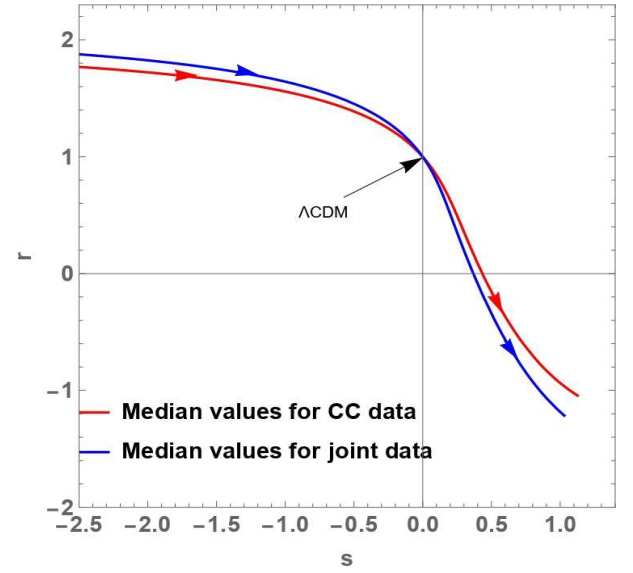


Figure 15: Model-II: Statefinder  $(r, s)$  trajectory.

## 6.5 Age of the Universe

The cosmic age  $t(z)$  of a cosmological model can be calculated in terms of the red-shift  $z$  as[78]:

$$t(z) = \int_z^\infty \frac{dz}{(1+z)H(z)}. \quad (38)$$

By using the Hubble parameter  $H(z)$  from equations (21) and (23), we calculate the present age of the universe for these models.

The age of the universe for model I is  $t_0$  (at  $z = 0$ ) =  $13.22_{-0.340}^{+0.165}$  Gyr (for the CC dataset) and  $t_0 = 13.41_{-0.46}^{+0.14}$  Gyr (for the joint data set). In model II, the present age of the universe is  $t_0 = 12.74_{-0.14}^{+0.18}$  Gyr and  $12.62_{-0.22}^{+0.33}$  Gyr for CC and joint data estimations respectively. We can see that the model's age of the universe has been change due to the absence of a structure formation era.

## 7 Conclusions

We study the universe evolution with the flat FLRW metric in  $f(R, L_m)$  gravity where the equation of state parameter for dark energy evolves reciprocal to the redshift in one case and varies exponentially in another case. These EoS parameters are popularly referred to as the Gong–Zhang parameterization and are given by  $\omega(z) = \frac{w_o}{z+1}$  and  $\omega(z) = \frac{w_o}{z+1} \exp\left(\frac{z}{z+1}\right)$ . The median value of model parameters are obtained using the MCMC analysis based on the observational data of CC and the supernovae type Ia Pantheon sample. The parameters are constrained through the MCMC analysis for both models and the results are summarized in Tables (1) and (2).

Moreover, the behaviour of deceleration parameters have been discussed. The evolution curve of the deceleration parameter reveals that the universe has transitioned from a decelerated to an accelerated expansion phase. For Model-I, the current values of deceleration parameters are  $q_0 = -0.60$  (CC) and  $q_0 = -0.59$  (joint) and the value of transition red-shift is  $z_t = 0.635$  (CC) and  $z_t = 0.71$  (joint). For Model II, the current value of deceleration parameter is obtain  $q = -0.2718$  and  $-0.4067$  for CC and joint data respectively. The value of transition red-shift is  $z_t = 0.7$  (CC) and  $z_t = 0.871$  (joint). The current value of the deceleration parameter is negative and it confirms the accelerated cosmic expansion in both models. These models are consistent with current observations of acceleration, but the early and late time dynamics may differ in these models. This is one of the important aspect of this study. The cosmological evolution in Model I progresses from early deceleration to the late-time super-exponential expansion. Unlike Model I, Model II exhibits no period of cold dark matter domination, resulting in the absence of a structure formation era. This model predicts the decelerating phase in the future, potentially resulting from energy exchange between dark energy and dark matter. Such a variation marks a key difference between both of these EoS parameterizations.

Additionally, we analyze the behavior of energy density and pressure. In Model-I, the energy density remains positive while the pressure starts with the positive values at high red-shift during the early universe and in current (and later epoch), it becomes negative. These findings are consistent with the accelerating universe's expanding behavior.

Figures (10) and (11) illustrate the behavior of EoS parameter for Model I and Model II, respectively. In model I, the value of EoS parameter at present is  $\omega = -0.801$  and  $\omega = -0.779$  for CC and joint data estimates respectively. Similarly, for model II,  $\omega = -0.768$  and  $\omega = -0.822$  for CC and joint data. Hence, it is clear that from Fig. (10) and (11) that these models exhibits quintessence behavior for dark energy at present times.

For Model I, the obtained age of the universe is  $t_0 = 13.22_{-0.340}^{+0.165}$  Gyr (CC) and  $t_0 = 13.41_{-0.46}^{+0.14}$  Gyr (joint) and for Model II, it is  $t_0 = 12.74_{-0.14}^{+0.18}$  Gyr (CC) and  $t_0 = 12.62_{-0.22}^{+0.33}$  Gyr (joint).

The difference between behaviors of Model I and Model II may be due to the  $\exp\left(\frac{z}{1+z}\right)$  term incorporated in Model II's EoS parameter. Because of this term, the cold dark matter dominated era is absent in the model II. As a consequence, key cosmological parameters such as the deceleration parameter and cosmic age of model II differs from those in the standard  $\Lambda$ CDM model and the model I.

## Acknowledgements

R. Garg thanks to Dr. A. Singh for the insightful discussions. G. P. Singh and F. Rahaman are thankful to the Inter-University Centre for Astronomy and Astrophysics (IUCAA), Pune, India for support under Visiting Associateship program.

## References

- [1] A. G. Riess, A. V. Filippenko, P. Challis, A. Clocchiatti, A. Diercks, et al., Observational Evidence from Supernovae for an Accelerating Universe and a Cosmological Constant, *Astronomical Journal* 116 (3) (1998) 1009–1038. doi:<https://doi.org/10.1086/300499>.
- [2] S. Perlmutter, G. Aldering, G. Goldhaber, R. A. Knop, P. Nugent, et al., Measurements of  $\Omega$  and  $\Lambda$  from 42 High-Redshift Supernovae, *Astrophysical Journal* 517 (2) (1999) 565–586. doi:<https://doi.org/10.1086/307221>.
- [3] N. Aghanim, Y. Akrami, M. Ashdown, J. Aumont, C. Baccigalupi, et al., Planck 2018 results. VI. Cosmological parameters, *Astronomy and Astrophysics* 641 (2020) A6. doi:<https://doi.org/10.1051/0004-6361/201833910>.
- [4] S. Weinberg, The cosmological constant problem, *Reviews of modern physics* 61 (1) (1989) 1. doi:<https://doi.org/10.1103/RevModPhys.61.1>.
- [5] E. Di Valentino, O. Mena, S. Pan, L. Visinelli, W. Yang, et al., In the realm of the hubble tension—a review of solutions, *Classical and Quantum Gravity* 38 (15) (2021) 153001. doi:<https://doi.org/10.1088/1361-6382/ac086d>.
- [6] S. M. Carroll, The cosmological constant, *Living reviews in relativity* 4 (1) (2001) 1–56. doi:<https://doi.org/10.12942/lrr-2001-1>.
- [7] R. Kerner, Cosmology without singularity and nonlinear gravitational Lagrangians., *General Relativity and Gravitation* 14 (5) (1982) 453–469. doi:<https://doi.org/10.1007/BF00756329>.
- [8] H. A. Buchdahl, Non-linear lagrangians and cosmological theory, *Monthly Notices of the Royal Astronomical Society* 150 (1) (1970) 1–8. doi:<https://doi.org/10.1093/mnras/150.1.1>.
- [9] S. Nojiri, S. D. Odintsov, Unified cosmic history in modified gravity: from  $f(r)$  theory to lorentz non-invariant models, *Physics Reports* 505 (2-4) (2011) 59–144. doi:<https://doi.org/10.1016/j.physrep.2011.04.001>.
- [10] S. Nojiri, S. D. Odintsov, V. K. Oikonomou, Modified gravity theories on a nut-shell: Inflation, bounce and late-time evolution, *Physics Reports* 692 (2017) 1–104. doi:<https://doi.org/10.1016/j.physrep.2017.06.001>.
- [11] T. Harko, F. S. Lobo, S. Nojiri, S. D. Odintsov,  $f(r, t)$  gravity, *Physical Review D* 84 (2) (2011) 024020. doi:<https://doi.org/10.1103/PhysRevD.84.024020>.

[12] Y.-F. Cai, S. Capozziello, M. De Laurentis, E. N. Saridakis,  $f(t)$  teleparallel gravity and cosmology, *Reports on Progress in Physics* 79 (10) (2016) 106901. doi:<https://doi.org/10.1088/0034-4885/79/10/106901>.

[13] S. Capozziello, V. Cardone, H. Farajollahi, A. Ravanpak, Cosmography in  $f(t)$  gravity, *Physical Review D* 84 (4) (2011) 043527. doi:<https://doi.org/10.1103/PhysRevD.84.043527>.

[14] S. Capozziello, R. D'Agostino, O. Luongo, Extended gravity cosmography, *International Journal of Modern Physics D* 28 (10) (2019) 1930016. doi:<https://doi.org/10.1142/S0218271819300167>.

[15] K. Bamba, S. D. Odintsov, L. Sebastiani, S. Zerbini, Finite-time future singularities in modified gauss-bonnet and  $f(r, g)$  gravity and singularity avoidance, *The European Physical Journal C* 67 (2010) 295–310. doi:<https://doi.org/10.1140/epjc/s10052-010-1292-8>.

[16] S. Capozziello, V. De Falco, C. Ferrara, The role of the boundary term in  $f(q, b)$  symmetric teleparallel gravity, *The European Physical Journal C* 83 (10) (2023) 915. doi:<https://doi.org/10.1140/epjc/s10052-023-12072-y>.

[17] G. P. Singh, A. R. Lalke, N. Hulke, Study of particle creation with quadratic equation of state in higher derivative theory, *Brazilian Journal of Physics* 50 (2020) 725–743. doi:<https://doi.org/10.1007/s13538-020-00788-1>.

[18] G. P. Singh, R. Garg, A. Singh, A generalized lambda cdm model with parameterized hubble parameter in particle creation, viscous and  $f(r)$  model framework, *International Journal of Geometric Methods in Modern Physics* (2025) 2550111 doi:<https://doi.org/10.1142/S0219887825501117>.

[19] R. Garg, G. P. Singh, A. Singh, Cosmic dynamics and observational constraints in  $f(q)$  gravity with affine equation of state, *arXiv preprint arXiv:2503.03212* (2025).

[20] G. K. Goswami, R. Rani, J. K. Singh, A. Pradhan, Flrw cosmology in weyl type  $f(q)$  gravity and observational constraints, *Journal of High Energy Astrophysics* 43 (2024) 105–113. doi:<https://doi.org/10.1016/j.jheap.2024.06.011>.

[21] N. Hulke, G. P. Singh, B. K. Bishi, A. Singh, Variable chaplygin gas cosmologies in  $f(r, t)$  gravity with particle creation, *New Astronomy* 77 (2020) 101357. doi:<https://doi.org/10.1016/j.newast.2020.101357>.

[22] A. Singh, Dynamical systems of modified gauss-bonnet gravity cosmological implications, *The European Physical Journal C* 85 (1) (2025) 1–12. doi:<https://doi.org/10.1140/epjc/s10052-024-13732-3>.

[23] K. N. Singh, G. R. P. Teruel, S. K. Maurya, T. Chowdhury, F. Rahaman, Conservative wormholes in generalized  $k(r, t)$ -function, *Journal of High Energy Astrophysics* 44 (2024) 132–145. doi:<https://doi.org/10.1016/j.jheap.2024.09.009>.

[24] T. Chowdhury, P. Rudra, T. Chowdhury, R. Farook, Study of wormhole in  $f(q)$  gravity with some dark energy models doi:<http://dx.doi.org/10.2139/ssrn.5065917>.

[25] A. Singh, S. Mandal, R. Chaubey, R. Raushan, Observational constraints on the expansion scalar and shear relation in the locally rotationally symmetric bianchi i model, *Physics of the Dark Universe* 47 (2025) 101798. doi:<https://doi.org/10.1016/j.dark.2024.101798>.

[26] S. Kotambkar, G. P. Singh, R. Kelkar, B. K. Bishi, Anisotropic bianchi type i cosmological models with generalized chaplygin gas and dynamical gravitational and cosmological constants, *Communications in Theoretical Physics* 67 (2) (2017) 222. doi:<https://doi.org/10.1088/0253-6102/67/2/222>.

[27] G. P. Singh, K. Desikan, A new class of cosmological models in lyra geometry, *Pramana* 49 (1997) 205–212. doi:<https://doi.org/10.1007/BF02845856>.

[28] M. B. Varela, O. Bertolami, Is cosmological data suggesting a nonminimal coupling between matter and gravity?, *Physics of the Dark Universe* 48 (2025) 101861. doi:<https://doi.org/10.1016/j.dark.2025.101861>.

[29] A. Singh, G. P. Singh, A. Pradhan, Cosmic dynamics and qualitative study of rastall model with spatial curvature, *International Journal of Modern Physics A* 37 (16) (2022) 2250104. doi:<https://doi.org/10.1142/S0217751X22501044>.

[30] G. P. Singh, A. R. Lalke, Cosmological study with hyperbolic solution in modified  $f(q, t)$  gravity theory, *Indian Journal of Physics* 96 (14) (2022) 4361–4372. doi:<https://doi.org/10.1007/s12648-022-02341-z>.

[31] A. Singh, R. Raushan, R. Chaubey, S. Mandal, K. C. Mishra, Lagrangian formulation and implications of barotropic fluid cosmologies, *International Journal of Geometric Methods in Modern Physics* 19 (07) (2022) 2250107. doi:<https://doi.org/10.1142/S0219887822501079>.

[32] A. Singh, Homogeneous and anisotropic cosmologies with affine eos: a dynamical system perspective, *The European Physical Journal C* 83 (8) (2023) 696. doi:<https://doi.org/10.1140/epjc/s10052-023-11879-z>.

[33] A. R. Lalke, G. P. Singh, A. Singh, Late-time acceleration from ekpyrotic bounce in  $f(q, t)$  gravity, *International Journal of Geometric Methods in Modern Physics* 20 (08) (2023) 2350131. doi:<https://doi.org/10.1142/S0219887823501311>.

[34] T. Harko, F. S. N. Lobo,  $f(r, l_m)$  gravity, *The European Physical Journal C* 70 (2010) 373–379. doi:<https://doi.org/10.1140/epjc/s10052-010-1467-3>.

[35] V. Faraoni, *Cosmology in scalar tensor gravity* (2004). doi:<https://doi.org/10.1007/978-1-4020-1989-0>.

[36] P. Zhang, Behavior of  $f(r)$  gravity in the solar system, galaxies, and clusters, *Physical Review D* 76 (2) (2007) 024007. doi:<https://doi.org/10.1103/PhysRevD.76.024007>.

[37] O. Bertolami, J. Páramos, S. G. Turyshhev, General theory of relativity: Will it survive the next decade?, in: *Lasers, Clocks and Drag-Free Control: Exploration of Relativistic Gravity in Space*, Springer, 2008, pp. 27–74. doi:<https://doi.org/10.48550/arXiv.gr-qc/0602016>.

[38] F. Rahaman, S. Ray, M. Kalam, M. Sarker, Do solar system tests permit higher dimensional general relativity?, *Int. J. Theor. Phys.* 48 (3) (2009) 3124–3138. doi:<https://doi.org/10.1007/s10773-009-0110-2>.

[39] S. Nojiri, S. D. Odintsov, Gravity assisted dark energy dominance and cosmic acceleration, *Physics Letters B* 599 (3-4) (2004) 137–142. doi:<https://doi.org/10.1016/j.physletb.2004.08.045>.

[40] G. Allemandi, A. Borowiec, M. Francaviglia, S. D. Odintsov, Dark energy dominance and cosmic acceleration in first-order formalism, *Physical Review D* 72 (6) (2005) 063505. doi:<https://doi.org/10.1103/PhysRevD.72.063505>.

[41] F. S. N. Lobo, T. Harko, Extended  $f(R, Lm)$  theories of gravity, 2015. doi:<https://doi.org/10.48550/arXiv.1211.0426>.

[42] Y. Myrzakulov, O. Donmez, G. D. A. Yildiz, E. Gudekli, S. Muminov, et al., Linear redshift parametrization of deceleration parameter in  $f(r, Lm)$  gravity, *Physics of the Dark Universe* 45 (2024) 101545. doi:<https://doi.org/10.1016/j.dark.2024.101545>.

[43] V. K. Bhardwaj, S. Ray, Cosmological model in the framework of  $f(r, lm)$  gravity with quadratic equation of state parameter, *Physics of the Dark Universe* (2025) 101930 doi:<https://doi.org/10.1016/j.dark.2025.101930>.

[44] L. V. Jaybhaye, R. Solanki, P. K. Sahoo, Late time cosmic acceleration through parametrization of hubble parameter in  $f(r, lm)$  gravity, *Physics of the Dark Universe* 46 (2024) 101639. doi:<https://doi.org/10.1016/j.dark.2024.101639>.

[45] S. Myrzakulova, M. Koussour, N. Myrzakulov, Investigating the dark energy phenomenon in  $f(r, lm)$  cosmological models with observational constraints, *Physics of the Dark Universe* 43 (2024) 101399. doi:<https://doi.org/10.1016/j.dark.2023.101399>.

[46] R. Garg, G. P. Singh, A. R. Lalke, S. Ray, Cosmological model with linear equation of state parameter in  $f(r, lm)$  gravity, *Physics Letters A* 525 (2024) 129937. doi:<https://doi.org/10.1016/j.physleta.2024.129937>.

[47] A. Pradhan, D. C. Maurya, G. K. Goswami, A. Beesham, Modeling transit dark energy in  $f(r, lm)$ -gravity, *International Journal of Geometric Methods in Modern Physics* 20 (06) (2023) 2350105. doi:<https://doi.org/10.1142/S0219887823501050>.

[48] B. K. Shukla, R. K. Tiwari, D. Sofuoğlu, A. Beesham, Flrw universe in  $f(r, lm)$  gravity with equation of state parameter, *East European Journal of Physics* (4) (2023) 376–389. doi:<https://doi.org/10.26565/2312-4334-2023-4-48>.

[49] D. C. Maurya, Bianchi-i dark energy cosmological model in  $f(r, lm)$ -gravity., *International Journal of Geometric Methods in Modern Physics* 21 (4) (2024). doi:<https://doi.org/10.1142/S0219887824500725>.

[50] A. Shukla, R. Raushan, R. Chaubey, Dynamical systems analysis of  $f(r, l, m)$  gravity model, *International Journal of Geometric Methods in Modern Physics* (2025) 2550118 doi:<https://doi.org/10.1142/S021988782550118X>.

[51] L. V. Jaybhaye, R. Solanki, S. Mandal, P. K. Sahoo, Cosmology in  $f(r, lm)$  gravity, *Physics Letters B* 831 (2022) 137148. doi:<https://doi.org/10.1016/j.physletb.2022.137148>.

[52] Y. Gong, Y.-Z. Zhang, Probing the curvature and dark energy, *Physical Review D* 72 (4) (2005) 043518. doi:<https://doi.org/10.1103/PhysRevD.72.043518>.

[53] J. Yang, X.-Y. Fan, C.-J. Feng, X.-H. Zhai, Latest data constraint of some parameterized dark energy models, *Chinese Physics Letters* 40 (1) (2023) 019801. doi:[10.1088/0256-307X/40/1/019801](https://doi.org/10.1088/0256-307X/40/1/019801).

[54] M. N. Castillo-Santos, A. Hernández-Almada, M. A. García-Aspeitia, J. Magaña, An exponential equation of state of dark energy in the light of 2018 cmb planck data, *Physics of the Dark Universe* 40 (2023) 101225. doi:<https://doi.org/10.1016/j.dark.2023.101225>.

[55] B. Ryden, *Introduction to cosmology* addison wesley san francisco (2003).

[56] T. Harko, F. S. N. Lobo, Generalized curvature-matter couplings in modified gravity, *Galaxies* 2 (3) (2014) 410–465. doi:<https://doi.org/10.3390/galaxies2030410>.

[57] T. Harko, F. S. N. Lobo, J. P. Mimoso, D. Pavón, Gravitational induced particle production through a nonminimal curvature–matter coupling, *The European Physical Journal C* 75 (2015) 1–15. doi:<https://doi.org/10.1140/epjc/s10052-015-3620-5>.

[58] D. Foreman-Mackey, D. W. Hogg, D. Lang, J. Goodman, emcee: the mcmc hammer, *Publications of the Astronomical Society of the Pacific* 125 (925) (2013) 306. doi:[10.1086/670067](https://doi.org/10.1086/670067).

[59] R. Jimenez, A. Loeb, Constraining cosmological parameters based on relative galaxy ages, *The Astrophysical Journal* 573 (1) (2002) 37. doi:<https://doi.org/10.1086/340549>.

[60] S. Mandal, A. Singh, R. Chaubey, Late-time constraints on barotropic fluid cosmology, *Physics Letters A* 519 (2024) 129714. doi:<https://doi.org/10.1016/j.physleta.2024.129714>.

[61] S. Mandal, A. Singh, R. Chaubey, Cosmic evolution of holographic dark energy in  $f(q, t)$  gravity, *International Journal of Geometric Methods in Modern Physics* 20 (05) (2023) 2350084. doi:<https://doi.org/10.1142/S0219887823500846>.

[62] A. Singh, S. Krishnannair, Affine eos cosmologies: Observational and dynamical system constraints, *Astronomy and Computing* 47 (2024) 100827. doi:<https://doi.org/10.1016/j.ascom.2024.100827>.

[63] D. M. Scolnic, D. O. Jones, A. Rest, Y. C. Pan, R. Chornock, et al., The complete light-curve sample of spectroscopically confirmed sne ia from pan-starrs1 and cosmological constraints from the combined pantheon sample, *The Astrophysical Journal* 859 (2) (2018) 101. doi:<https://doi.org/10.3847/1538-4357/aab9bb>.

[64] A. G. Riess, R. P. Kirshner, B. P. Schmidt, S. Jha, P. Challis, et al., BVRI light curves for 22 type ia supernovae, *The Astronomical Journal* 117 (2) (1999) 707. doi:<https://doi.org/10.1086/300738>.

[65] M. Hicken, W. M. Wood-Vasey, S. Blondin, P. Challis, S. Jha, et al., Improved dark energy constraints from 100 new cfa supernova type ia light curves, *The Astrophysical Journal* 700 (2) (2009) 1097. doi:<https://doi.org/10.1088/0004-637X/700/2/1097>.

[66] M. Sako, B. Bassett, A. C. Becker, P. J. Brown, H. Campbell, et al., The data release of the sloan digital sky survey-ii supernova survey, *Publications of the Astronomical Society of the Pacific* 130 (988) (2018) 064002. doi:[10.1088/1538-3873/aab4e0](https://doi.org/10.1088/1538-3873/aab4e0).

[67] J. Guy, M. Sullivan, A. Conley, N. Regnault, P. Astier, et al., The supernova legacy survey 3-year sample: Type ia supernovae photometric distances and cosmological constraints, *Astronomy & Astrophysics* 523 (2010) A7. doi:<https://doi.org/10.1051/0004-6361/201014468>.

[68] C. Contreras, M. Hamuy, M. M. Phillips, G. Folatelli, N. B. Suntzeff, et al., The carnegie supernova project: first photometry data release of low-redshift type ia supernovae, *The Astronomical Journal* 139 (2) (2010) 519. doi:[10.1088/0004-6256/139/2/519](https://doi.org/10.1088/0004-6256/139/2/519).

[69] S. D. Odintsov, V. Oikonomou, A. Timoshkin, E. N. Saridakis, R. Myrzakulov, Cosmological fluids with logarithmic equation of state, *Annals of Physics* 398 (2018) 238–253. doi:<https://doi.org/10.1016/j.aop.2018.09.015>.

- [70] G. F. R. Ellis, R. Maartens, M. A. MacCallum, *Relativistic cosmology*, Cambridge University Press, 2012.  
doi:<http://dx.doi.org/10.1017/CBO9781139014403>.
- [71] K. Asvesta, L. Kazantzidis, L. Perivolaropoulos, C. G. Tsagas, Observational constraints on the deceleration parameter in a tilted universe, *Monthly Notices of the Royal Astronomical Society* 513 (2) (2022) 2394–2406. doi:<https://doi.org/10.1093/mnras/stac922>.
- [72] A. R. Lalke, G. P. Singh, A. Singh, Cosmic dynamics with late-time constraints on the parametric deceleration parameter model, *The European Physical Journal Plus* 139 (3) (2024) 288. doi:<https://doi.org/10.1140/epjp/s13360-024-05091-5>.
- [73] S. Chakraborty, S. Pan, S. Saha, A third alternative to explain recent observations: Future deceleration, *Physics Letters B* 738 (2014) 424–427. doi:<https://doi.org/10.1016/j.physletb.2014.10.009>.
- [74] A. A. Escobal, J. F. Jesus, S. H. Pereira, J. A. S. Lima, Can the universe decelerate in the future?, *Physical Review D* 109 (2) (2024) 023514. doi:<https://doi.org/10.1103/PhysRevD.109.023514>.
- [75] M. Visser, Energy conditions in the epoch of galaxy formation, *Science* 276 (5309) (1997) 88–90. doi:<https://doi.org/10.1126/science.276.5309.88>.
- [76] V. Sahni, T. D. Saini, A. A. Starobinsky, U. Alam, Statefinder—a new geometrical diagnostic of dark energy, *Journal of Experimental and Theoretical Physics Letters* 77 (2003) 201–206. doi:<https://doi.org/10.1134/1.1574831>.
- [77] U. Alam, V. Sahni, T. Deep Saini, A. A. Starobinsky, Exploring the expanding universe and dark energy using the statefinder diagnostic, *Monthly Notices of the Royal Astronomical Society* 344 (4) (2003) 1057–1074. doi:<https://doi.org/10.1046/j.1365-8711.2003.06871.x>.
- [78] M.-L. Tong, Y. Zhang, Cosmic age, statefinder, and om diagnostics in the decaying vacuum cosmology, *Physical Review D* 80 (2) (2009) 023503. doi:<https://doi.org/10.1103/PhysRevD.80.023503>.